JOURNAL OF GEOPHYSICAL RESEARCH, VOL. 92, NO. C2, PAGES 1899–1913, FEBRUARY 15, 1987

Modeled Surface Dynamic Height in 1964–1984: An Effort to Assess How Well the Low Frequencies in the Equatorial Atlantic Were Sampled in 1982–1984

GILLES REVERDIN

Laboratoire d'Océanographie Dynamique et de Climatologie, Centre National de Recherche Scientifique, Paris

YVES DU PENHOAT

Office de la Recherche Scientifique et Technique d'Outre-Mer, Centre Océanographique de Bretagne, Brest, France

A wind-forced linear model has been used to produce 21 years (1964–1984) of monthly time series of surface dynamic height in the equatorial Atlantic. The climatological seasonal cycle is subtracted, and the statistical characteristics of the residuals are analyzed. An empirical orthogonal function analysis reveals that the most significant pattern has deviations of one sign in the western equatorial Atlantic associated with near-simultaneous deviations of the opposite sign in the eastern equatorial Atlantic. The anomalies in the last 2 years, 1983 and 1984, are particularly large. The time component of the first empirical orthogonal function peaks in July 1983, changes sign at the end of 1983, and has an extremum of the opposite sign in April 1984. At that time, the zonal slope of dynamic height had reversed with respect to normal along the equator. In 1983–1984 a large data set was collected to study the seasonal variability in the equatorial Atlantic. We do not analyze the real data here but evaluate the ability of this data set to cover correctly the time and space scales of the modeled anomalies. The model time series are sampled at the positions of the data. An optimal interpolation scheme is used with the adequate statistics extracted from the model time series, and the analysis is compared with the simulation. Our results suggest that the most noticeable features of the model anomalies for 1983–1984 are reproduced in the analysis, although the results would have been better if more data had been collected in the western equatorial Atlantic at the end of 1983. According to this study, subsets which have already been analyzed for the same period (for example, the Programme Français Ocean Climat dans l'Atlantique Equatorial conductivity-temperature-depth cruises) would also have retained the reversal of sign of the anomaly between the end of 1983 and early 1984, although the overall accuracy would have been reduced.

1. INTRODUCTION

The upper tropical Atlantic density structure has a large low-frequency variability revealed by analyses of the historical data files. Along the equator the zonal tilt of surface dynamic height or of other related parameters is usually weakest in April–May and strongest in July [*Merle*, 1978, 1980; *Katz et al.*, 1977; *Katz*, 1981; *Merle and Arnault*, 1985], and the slope across the North Equatorial Countercurrent (NECC) between 3°N and 9°N is maximum in September [*Garzoli and Katz*, 1983]. The information originates from isolated cruises, and there are few regional or global surveys to cover this variability (examples of such limited surveys are given by *Katz et al.* [1977], *Lass et al.* [1983], *Molinari et al.*, [1986], and *Reverdin et al.* [1986]). Compositing such data to form a seasonal cycle can be misleading [*Houghton*, 1983], and the need to have an adequate coverage of the tropical Atlantic over more than one seasonal cycle motivated the buildup of the French-U.S. cooperative Programme Français Océan Climate dans l'Atlantique Tropical (FOCAL)/Seasonal Response of the Equatorial Atlantic (SEQUAL) [*Weisberg*, 1984]. To achieve these experimental goals, two sets of data have been collected, mainly between March 1983 and October 1984: for the first one, continuous records were available for a limited number of places east of 38°30'W, primarily along the equator or north of it; for the second one, sections have been performed in various areas usually along prescribed lines (Figure 1). The two data sets are expected to be complementary in the future: the time series are required to suggest the variability in which the sections are embedded, and the sections should provide spatial information, at least for the low frequencies.

The FOCAL-SEQUAL array was designed in order to provide ground truth for numerical models previously forced with climatological winds (*Busalacchi and Picaut* [1983], *du Penhoat and Tréguier* [1985] (hereinafter referred to as PT), or *Philander and Pacanowski* [1984, 1986] with *Hellerman and Rosenstein* [1983] wind stresses). The skill of the models will be tested against the available data. One is particularly interested in knowing whether or not the low-frequency variability of the Atlantic Ocean is correctly hindcasted by the numerical models. High frequencies should also be carefully assessed in the data in order to estimate their effect on the seasonal cycle. Validation of the hindcasts could be done in a few locations where long time series are available. In addition, it is necessary to estimate whether or not these places are characteristic of the large scale variability in the equatorial Atlantic. In principle, this could be investigated with the whole FOCAL-SEQUAL data set. However, these data are not yet available. A preliminary question that is addressed here is whether or not the FOCAL-SEQUAL array resolves adequately the characteristic time and space scales of the seasonal cycle.

If enough data were available in the past, one could define the characteristic scales of the seasonal cycle from the observations. Unfortunately, this is not the case, mainly because previous experiments (GARP Atlantic Tropical Experiment (GATE) [*Düing et al.*, 1980] or First GARP Global Experiment (FGGE) [*Molinari et al.*, 1986]) have not lasted long enough to cover the seasonal cycle. In the absence of real data, we will rely on a model for investigating the scales of the seasonal cycle and to provide realizations of the variability with which the performance of the analysis can be tested. What

Copyright 1987 by the American Geophysical Union.

Paper number 6C0617.
0148-0227/87/0

Fonds Documentaire ORSTOM
010006323

Fonds Documentaire ORSTOM
Cote : B* 6323 Ex : 1

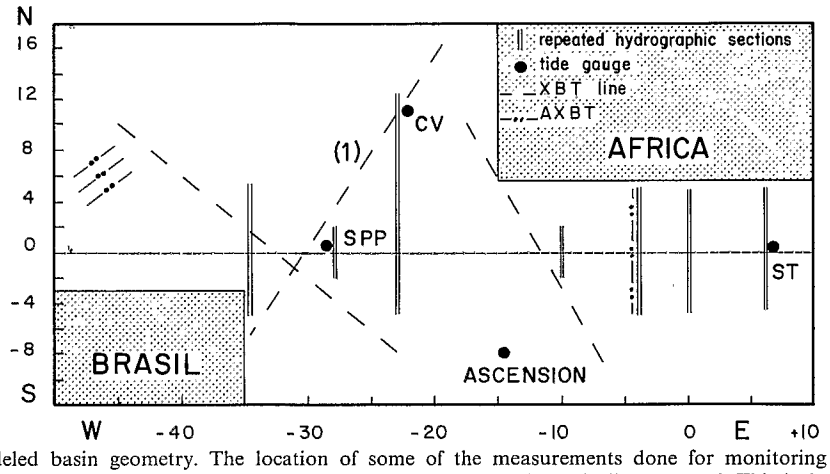

Fig. 1. Modeled basin geometry. The location of some of the measurements done for monitoring the equatorial Atlantic density structure during FOCAL/SEQUAL in 1983–1984 are schematically presented. This includes XBTs (note that XBT line 1 running NE to SW is the most heavily sampled, with 2 to 4 sections per month), AXBTs, and the FOCAL cruise CTDs (repeated hydrographic sections).

we call a model is a multiyear numerical simulation, and it should be interpreted in a statistical sense. Our conclusions are dependent on the properties of the model, which may differ from the ones of the real ocean: an investigation of the validity of the model with a subset of the FOCAL data will be presented in another paper. Although we do not know how realistic such multiyear wind forced simulations are, we have some hints that some of the model properties are realistic: the numerical scheme which represents a linear low-frequency ocean with a prescribed vertical density profile [PT] has reproduced most aspects of the climatological surface dynamic height topography presented by *Arnault* [1984] and *Merle and Arnault* [1985]. Models with similar assumptions have also produced correct hindcasts in multiyear simulations of tide gauge records in the equatorial Pacific Ocean [*Busalacchi and O'Brien*, 1981; *Busalacchi and Cane*, 1985]. No long time series of sea level are yet available in the tropical Atlantic, and the parameter on which we will restrict our investigation is the surface dynamic height referred to 500 dbar. FOCAL-SEQUAL data from which it could be estimated are numerous (Figure 1):

1. It is readily available from hydrographic sections [*Hisard and Hénin*, 1984].
2. Via *T-S* relations, it is likely to be extracted from temperature profiles (expendable bathythermographs (XBTs) or aircraft expendable bathythermographs (AXBTs) with enough accuracy [*Arnault*, 1984].
3. Low frequencies in tide gauge pressure records may also be included near the equator according to comparisons with hydrographic sections [*Katz et al.*, 1986].
4. Finally, "inverted echo sounders" transit time is probably also a good proxy for dynamic height [*Katz*, 1987].

To investigate the performances of the array, we will construct analyzed fields using "optimal interpolation" of data extracted from the model simulations and will compare these analyses with the simulations. The organization of the paper is the following. In section 2, we present the numerical model of the tropical Atlantic and the wind forcing from which a 21-year-long hindcast of the surface dynamic topography is derived. Time series are presented. In section 3, an outline of the analysis method is given to define which statistics are needed from the hindcast. In section 4, the statistics of the model simulations are discussed. Two questions are asked: how does 1983–1984 compare with respect to the 21-year time series, and what are the statistical characteristics of the deviations from the mean seasonal cycle? In section 5, proxy data are created from the model at the locations of the FOCAL-SEQUAL data. They are analyzed to produce grid fields h_a. These fields are compared with the model values h_s. Section 6 contains a discussion of the results with regard to the FOCAL-SEQUAL experiment.

2. Model Hindcast (1964–1984)

2.1. *The Numerical Model*

The model is a linear wind-forced model of a stratified ocean of depth h and has been described by PT. Briefly, to solve the equations, the vertical density profile is linearized about a mean state $\rho(z)$ (or a Brunt-Väisälä frequency $N(z)$) estimated from the climatology [*Merle*, 1978]. This results in a decomposition into vertical modes [*Lighthill*, 1969], such as

$$(u, v, p) = \sum_n (u_n, v_n, p_n)(x, y, t)H_n(z) \tag{1}$$

where x, y are zonal and meridional cordinates in the equatorial β plane and the orthonormal vertical modes $H_n(z)$ are the solutions of the eigenfunction equation

$$d/dz\ (1/N^2\ dH_n/dz) + (1/{c_n}^2)H_n = 0 \tag{2}$$

with $dH_n/dz = 0$ at $z = 0$ and $z = -D$, D being the depth of the ocean and c_n the phase speed associated with mode n. For each baroclinic mode ($n \geq 1$), the horizontal equations are written in the long-wave approximation [*Cane and Sarachik*, 1981]

$$u_{n,t} - \beta y v_n + p_{n,x} = {\tau_n}^x - r_n u_n \tag{3a}$$

$$\beta y u_n + p_{n,y} = {\tau_n}^y - r_n v_n \tag{3b}$$

$$1/{c_n}^2 p_{n,t} + u_{n,x} + v_{n,y} = -r_n/{c_n}^2 p_n \tag{3c}$$

where r_n are damping coefficients and ${\tau_n}^x$ and ${\tau_n}^y$ are projections of the wind forcing onto the vertical modes. With this set of equations, western boundaries are not explicitely solved, but the solution has a simple analytical formulation which allows for an efficient numerical procedure [*Cane and Patton*, 1984]. It separates eastward (Kelvin mode) and westward (long Rossby modes) energy propagations. The Kelvin wave

contribution is solved along characteristics, and the long Rossby waves are computed with an implicit finite difference scheme which is unconditionally stable [*Cane and Patton*, 1984]. Thus we can use a 10-day time step, and the model is run cheaply for long simulations.

The physics included in r_n is not well known (see discussions by *McCreary* [1981] and *Gent et al.* [1983]). Here the dependence of r_n on mode number n has been chosen as by *McCreary* [1981] and corresponds to a 2-year decay time for the first vertical mode as in the work of *Gent et al.* [1983]. PT showed in their multimode simulation of surface dynamic height that near the equator, with a similar choice for damping, the first three modes accounted for 95% of the seasonal signal estimated with 9 modes. Hence only the first three baroclinic modes are numerically solved (speeds of $c_1 = 2.16$ m s^{-1}, $c_2 = 1.26$ m s^{-1}, and $c_3 = 0.91$ m s^{-1}). Then sea surface dynamic height referred to 500 dbar is computed from the p_n as given by PT.

Wave propagation is nondispersive in the model, an approximation which is adequate only close to the equator. The wavelike patterns (wavelengths of the order of 4°.) found in the simulations at latitudes higher than 10° are probably not relevant for the dispersive dynamics of the ocean. The model geometry is shown in Figure 1. It is a rectangular basin except for steps in Brazil and western Africa. The grid step is 1° in the zonal and 0.5° in the meridional direction. In the real ocean, there are no coastlines at 12°S and 18°N, nor is there a western boundary at 50°W north of the equator. However, with the damping chosen (2 years for the first mode), this does not influence significantly the equatorial band.

A requirement for numerical experiments at low frequencies is that mass (and therefore, here, dynamic height) should be conserved. The scheme conserves mass and energy in the interior in the absence of forcing and damping [*Cane and Patton*, 1984]. However, losses on the boundaries through wave reflection are likely. They are, however, very small, and mass is nearly conserved in the simulation.

2.2. *The Winds*

Monthly wind stress maps [*Servain et al.*, 1985] were first constructed for the period 1964–1979 on a 2° × 2° grid mesh with a "successive correction" objective analysis of ship reports averaged in 5°. × 2° boxes. Prior to the analysis, bogus data were added in data-void areas by a chief analyst as was done by *Legler and O'Brien* [1985]. Details on the processing of these winds are given by *Picaut et al.* [1985]. Recently, the processing has been changed slightly and the analysis has been rerun producing a time series from 1964 until 1984, including the FOCAL-SEQUAL field experiment phase. The accuracy of these wind stresses is not provided, but they generally incorporate a large number of data (over 5000 per month in the study area). Our concern with these data is to know their ability to reproduce the low-frequency variability. For example, there is an increase in wind intensity lasting until 1980, followed by a plateau. Some of these changes are instrument related [*Kaufeld*, 1981]. Also, high frequencies will be aliased into lower frequencies after sampling at midmonth of a monthly running mean–filtered series, a possible problem if the 40- to 50-day oscillations are energetic [*Madden and Julian*, 1972].

The wind field in the tropical Atlantic exhibits a strong seasonal signal. The intertropical convergence zone (ITCZ) separating the prevailing northeast and southeast trade winds

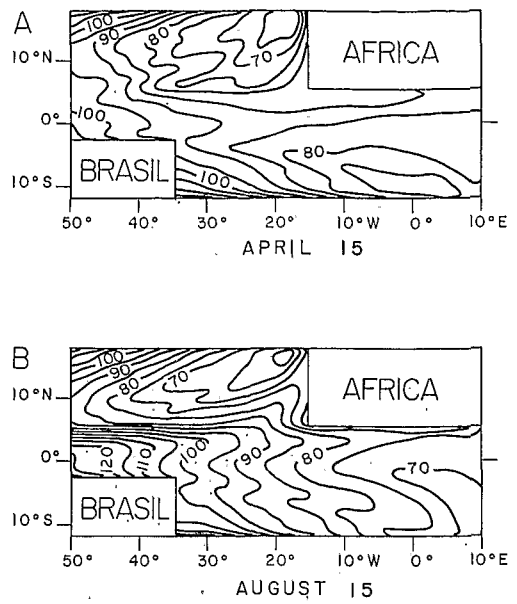

Fig. 2. Model mean seasonal cycle of dynamic height referred to 500 dbar for the years 1964–1984. Maps of the dynamic height topography (in dynamic centimeters) are presented (*a*) for April 15 and (*b*) for August 15.

straddles the equator in boreal winter and migrates northwards around May to reach its northernmost location around August (by 10°N near Africa) [*Hastenrath*, 1984]. Year-to-year variations of these displacements are observable. For example, in early 1983 the ITCZ stayed north of the equator at a latitude higher than that normally found and moved to the north beginning in mid-April, whereas in 1984 it stayed in the vicinity of the equator for a long period which was followed beginning in mid-May by a fast northward migration. For the 1964–1984 period, the strongest anomalies reported by *Servain et al.* [1985] occurred in May 1968, when a reversal of the equatorial winds took place [*Servain*, 1984].

Servain et al. [1985] quantified the wind anomalies (by anomalies, we refer to deviations from the mean seasonal cycle). Over large portions of the equatorial Atlantic, monthly anomalies of the wind stress have a variance larger than that in the climatological seasonal cycle. North of the equator, where the seasonal cycle is large, the anomalies have a smaller variance than the climatological seasonal cycle. Their analysis also suggests that anomalies are phase locked with the seasonal cycle, although they may last in some instances over more than a year.

2.3. *The Simulation of Dynamic Height*

Wind stresses are computed from the winds $\mathbf{V}$ as $\rho c_d |V| \mathbf{V}$, where c_d is chosen as 1.5×10^{-3} and $\rho = 1.2$ kg m^{-3}. The wind stresses are interpolated linearly in time at each model time step, every 10 days and spatially at the model grid points as described by PT. The model is spun up during 10 years with the mean seasonal cycle of the wind forcing. Then the simulation is continued with the 21-year-long wind stress time series as input. Since the pre-1964 period has no influence on the simulated dynamic height, the initial conditions influence the first year of the simulation [*Cane*, 1979; *Philander and Pacanowski*, 1980].

In a simulation a 21-year-long time series of dynamic height (January 1964 to December 1984) is produced that we sample at midmonth. The mean seasonal cycle of dynamic height in

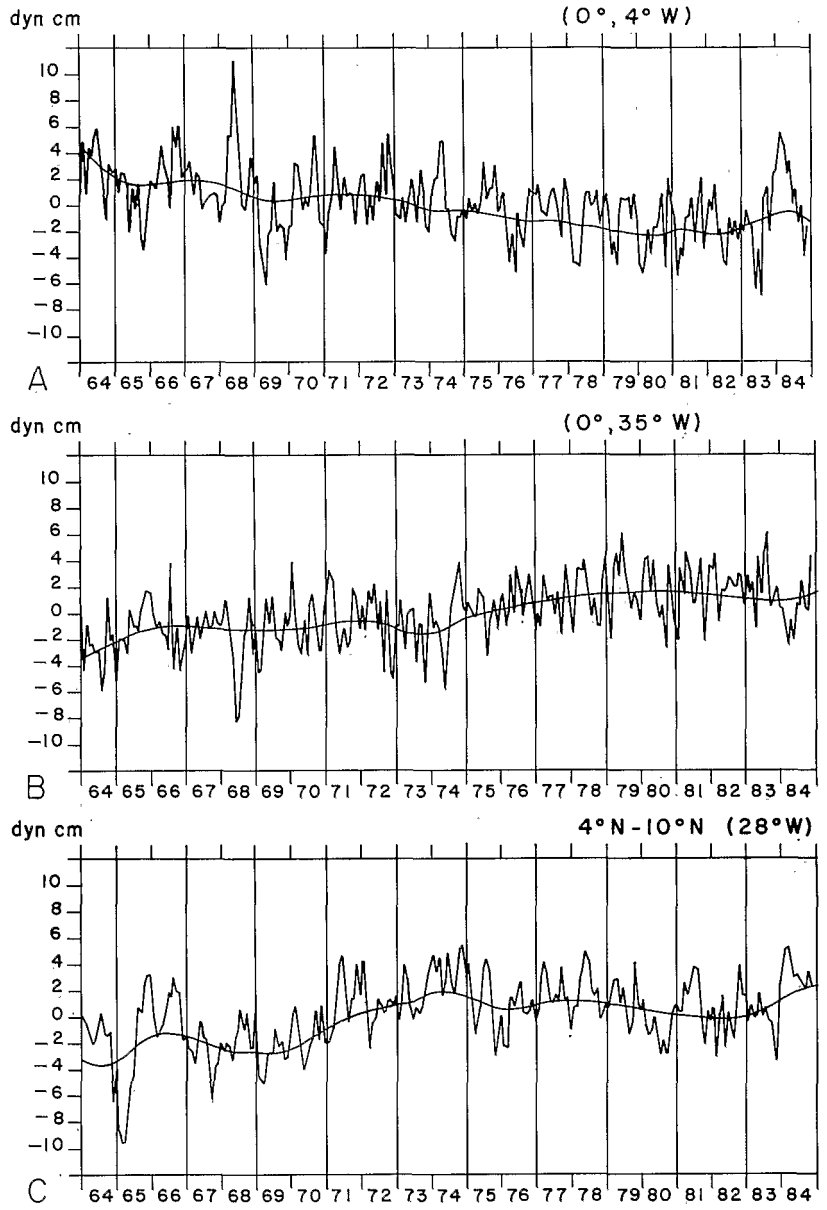

Fig. 3. The time series of the model dynamic height anomalies sampled at each midmonth. The mean seasonal cycle has been removed from the model outputs, and the low frequencies which are subsequently subtracted from the time series are also shown (solid line). Plots are for (0°, 4°W), (*b*) (0°, 35°W), and (*c*) the differences of dynamic height at 4°N–10°N along 28°W.

this simulation bears a close resemblance to the one obtained by PT with 9 vertical modes forced by *Hellerman and Rosenstein*'s [1983] climatology. The main difference is that the seasonal cycle is slightly more intense here. Two characteristic months of the seasonal cycle (April and August) are shown (Figure 2). In these fields, as in the climatology of dynamic height estimated from observations [*Merle and Arnault*, 1985], it is in April that the topography is the weakest and in July–August that it is most well formed with a trough (low pressure) near 10°N, a ridge (high pressure) near 3°N in the central and western Atlantic Ocean, and an equatorial trough with a strong downward slope toward the east.

Anomalies are computed by removing from the simulations the average seasonal cycle. In most places, a large trend is present (Figure 3), as is found in the wind stresses. Then we remove the trend as well as the lowest frequencies, which are most sensible to changes in wind measurement techniques [*Kaufeld*, 1981] and to the presence of the artificial meridional walls of the model. A low-pass second-order Butterworth recursive filter [*Murakami*, 1979] with a cutoff at 5 years is applied to the time series. This leaves a significant year-to-year variability accounting everywhere for more than two thirds of the variances in the anomalies. The small scales at high latitudes, where dynamics are poorly taken into account by the model, are also smoothed with weights $\frac{1}{4}$, $\frac{1}{2}$, $\frac{1}{4}$ for neighboring grid points separated by 2° in the zonal direction and 1° in the meridional direction. This has little effect closer to the equator, but 10° off the equator it strongly reduces the variance. After this smoothing, the outputs are subsampled on a 2° by 4° latitude-longitude mesh, and grid points over the continent are eliminated, resulting in filtered fields with 166 grid points, as is presented on in Figure 9.

Very few large-scale surveys have been performed previous to FOCAL/SEQUAL with which the model can be compared, so that we will consider here only the model simulations.

2.4. *Anomaly Time Series*

Time series of the unfiltered anomalies are shown (Figure 3) in two places along the equator: 4°W, which has been usually chosen to discuss the equatorial upwelling [*Houghton*, 1983; *Picaut*, 1983], and 35°W, which is in the western Atlantic where the wind seasonal cycle is the most intense. The variations at these two places are characteristic of those observed in the eastern and western equatorial Atlantic, although amplitudes are large in places closer to the boundaries. The anomalies are weaker in the central equatorial Atlantic, at 28°W for example. The strongest anomalies are found in 1968, as is also the case in a simulation for 1964–1979 depicted by *Servain et al.* [1985]. The years 1983 and 1984 have anomalies of comparable amplitudes, and the anomalies exceed 2 standard deviations in most locations for more than 3 months in a row for both of these years. Anomalies in 1984 bear similarities to those in 1968, but they occur earlier in 1984 by about 2 months, peaking in April. A reversal of the equatorial slope even occurred for these years: in May–June 1968 and in March–April 1984, the modeled dynamic height was lower at 35°W than at 4°W. Anomalies in 1983 have the opposite sign (the simulation in 1983–1984 is also discussed by *du Penhoat and Gouriou* [1987]). Quite often, anomalies of opposite signs are grouped in 2 successive years (for the winds, similar evidence for quasi-biennial oscillations is presented by *Servain et al.* [1985]). The variance of the anomalies, averaged spatially over the domain and temporally over 2 years, also shows large variations. It is larger between 1968 and 1972 and in 1983–1984 and smaller at other times (σ_m in Fig. 13).

The deviations of the meridional slope $h_{4°N}$–$h_{10°N}$ at 28°W are also presented (Figure 3c). The meridional slope has a seasonal cycle described by *Garzoli and Katz* [1983]. Its deviations suggest variations of the strength of the North Equatorial Countercurrent. They can be large, especially in 1965 when the slope is weaker than normal. Anomalies at the end of 1983 show a weakening of the slope and in the earlier part of 1984 a strengthening. These anomalies are always small compared to the huge seasonal cycle which takes place in that area (it exceeds 20 dyn cm peak-to-peak).

3. AN OUTLINE OF THE ANALYSIS

The model time series are cut into segments of length T (for example, 2 years, to simulate the duration of the FOCAL-SEQUAL experiment). Each segment is considered as one realization of the variability, and (x, t) is a space-time coordinate within the segment. We can write the model dynamic height h_s as

$$h_s(x, t) = \sum_{m=1}^{p} a_m L_m(x, t) + \mathrm{Res}_p(x, t) \tag{4}$$

where $\{L_m\}$ form a set of p orthonormal functions and a_m are projections on these functions. These functions define a subspace which we will refer to as the signal, and Res_p is a residual.

At n positions (x_i, t_i) (the array), proxy data (d_i) are extracted from the model, adding a term Err_i for errors and unresolved scales:

$$d_i = \sum_{m=1}^{p} a_m L_m(x_i, t_i) + \mathrm{Res}_p(x_i, t_i) + \mathrm{Err}_i \tag{5}$$

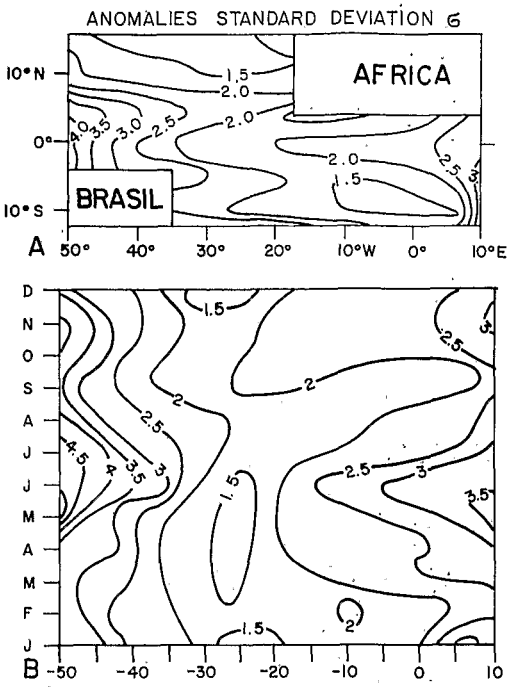

Fig. 4. Standard deviations σ of the anomalies (in dynamic centimeters): (*a*) rms deviation in the time series of detrended anomalies (see Figure 3) and (*b*) seasonal cycle along the equator.

The three terms in the right-hand side of (5) will be assumed to be statistically independent (this is obvious for the first and second terms and is assumed for the first and third terms). Also, if data are subsampled adequately, the last two terms will be uncorrelated between different data and will be referred to as a noise with variance σ^2. Now, we want to estimate optimally the signal h_a from the data, that is, find the most likely set $\{\hat{a}_m\}$ for the projections on $\{L_m\}$

$$h_a(x, t) = \sum_{m=1}^{p} \hat{a}_m L_m(x, t) \tag{6}$$

The most efficient (and the cheapest) way to perform the analysis is when a_m are joint normally distributed variables with zero mean and known expected variances A_m, i.e.,

$$\langle a_m \rangle = 0 \qquad \langle a_m a_n \rangle = A_{mn} = A_m \delta_{m,n} \tag{7}$$

where the angle brackets indicate an average over the different realizations. Then for one given realization and a prescribed data distribution (the array), the most likely $\{\hat{a}_m\}$ are obtained [*Bretherton et al.*, 1984; *McPhaden et al.*, 1984*a*] as a solution of:

$$\sum_{m=1}^{p} (A_{mn} + R_{mn})\hat{a}_m = S_n \tag{8}$$

where

$$R_{mn} = \sum_i L_n(x_i, t_i) 1/\sigma_i^2 \, L_m(x_i, t_i)$$

$$S_n = \sum_i L_n(x_i, t_i) 1/\sigma_i^2 \, d_i$$

and the estimated error covariance matrix of the $\hat{a}_m$ is $[(A) + (R)]^{-1}$.

To have a zero mean $\langle a_m \rangle$, the time average of the simulation over the 21 years is removed. To insure that different realisations are independent, we also have to subtract a mean

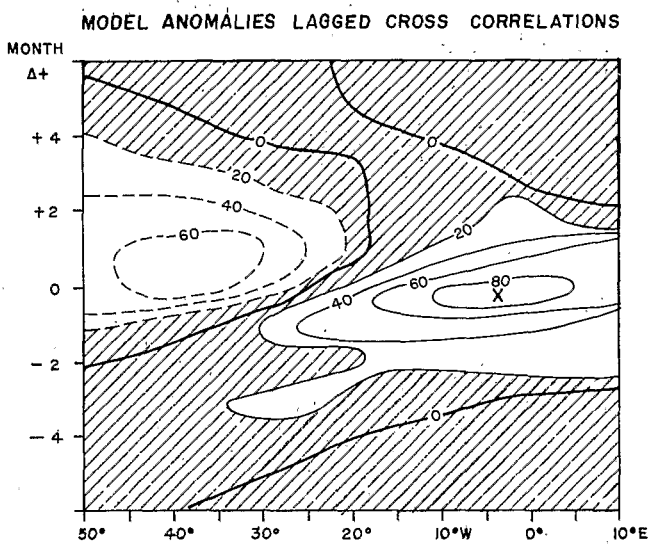

Fig. 5. Lagged cross-correlations $C(\Delta t, x) = \overline{h(t, 4°\text{W})\, h(t + \Delta t, x)}$, where the overbar denotes an average over time t, and h are anomalies normalized to unity. The reference point is at 4°W (cross). The hatched zones indicate correlations not significantly different from zero at the 90% confidence level.

seasonal cycle, and in this paper, we will work only with the deviations from the seasonal cycle. The requirement $\langle a_m a_n \rangle = 0$ for m different than n is equivalent to choosing $\{F_m\}$ as the empirical orthogonal functions (EOFs) of the system [*Lorenz*, 1956]. This can be seen by considering the covariance matrix $[C]$, which has elements:

$$C(x, t; x', t') = \langle h_a(x, t) h_a(x', t') \rangle \tag{9}$$

with (x, t), (x', t') being two grid points. It simplifies with the substitution of (4) to:

$$C(x, t; x', t') = \sum_{m=1}^{P} A_m F_m(x, t) F_m(x', t') \tag{10}$$

Then one can show that

$$[C] F_m = A_m F_m \tag{11}$$

The reciprocal is easy to prove. Extracting the useful statistical information from the model consists therefore of estimating the eigenvalues of the covariance matrix and their associated eigenfunctions.

4. Statistics of the Model

4.1. *Variance and Correlations*

The standard deviation of the anomalies (Figure 4*a*) is strongest in the eastern and in the western equatorial Atlantic, with weaker anomalies in the central Atlantic Ocean. They are also weaker at 10°N, where they are smaller than the standard deviation in the climatological seasonal cycle. The spatial distribution is slightly different from that presented by *Servain et al.* [1985]. In the Gulf of Guinea (0° to 20°W) their model exhibits smaller anomalies near the equator than further south. This differs from our model and is typical of the disagreements which were also found when discussing the climatology [*Busalacchi and Picaut*, 1983; PT].

Servain et al. [1985] suggested that the wind anomalies were seasonally dependent, and this also appears in the wind-forced simulation of dynamic height (Figure 4*b*). The rms standard deviation of the anomalies is weaker near the equator from January until April and from August through November. In April there is also very little meridional structure. In May to July, deviations are much larger near the equator (as is also found in the winds [*Picaut et al.*, 1985]. Note also that along the equator, maximum standard deviations in the east lead by 2 weeks a maximum in the west. In the central Atlantic, deviations are much smaller. The equatorial maximum in the east is most pronounced in June. However, differences between months are only marginally significant, considering that there are 21 years and assuming that two successive seasons are independent realizations.

The seasonal cycle in the Gulf of Guinea has been the source of many investigations. One major question was whether or not changes east of 15°W could be traced to causes in the western Atlantic. *Moore et al.* [1978], *McCreary et al.* [1983], and *Busalacchi and Picaut* [1983] have suggested that the equatorial Gulf of Guinea is responding to changes in the wind fields of the western Atlantic Ocean. The details of the effects of the wind structure and the response in the Gulf of Guinea have also been reviewed by *Weisberg and Tang* [1985]. For the model, the question to be asked is whether or not eastward propagating anomalies can be found. The numerical model is linear, and it is possible to interpret separately the deviations from the mean seasonal cycle. We consider lagged cross correlations along zonal equatorial sections, as $C(x, \Delta t) = \overline{r_s(x, t_0 + \Delta t) r_s(x_0, t_0)}$, where x_0 is a specified longitude reference along the equator, the overbar denotes the average over t_0, and r_s are the model anomalies normalized by their standard deviation. This was also done by *Busalacchi and O'Brien* [1981] to interpret the interannual variability of the Pacific Ocean. Correlations after 3 months are positive but small and are not significant (95% confidence levels for nonzero correlation are indicated in Figure 5 with the assumption that the correlation time scale is 3 months (80 degrees of freedom)). With a reference in the eastern Atlantic at 4°W (Figure 5), the most significant pattern suggests almost simultaneous anomalies of the opposite sign in the western Atlantic. The pattern of positive correlation extends also to the west with a lead of 2 months at 35°W. To moderate these results, notice that the positive correlations are weak west of 25°W

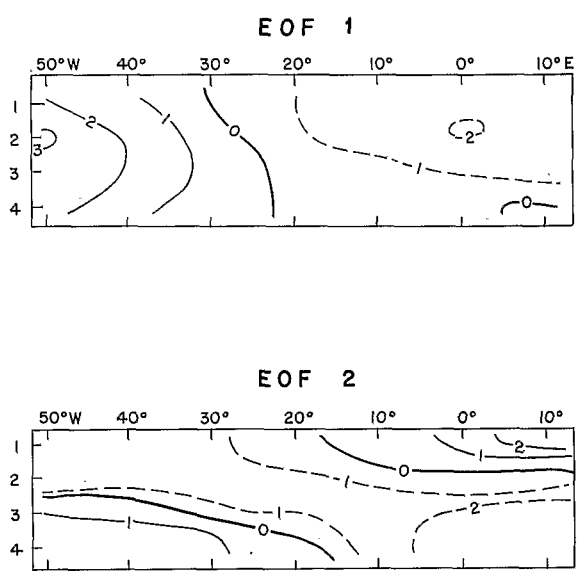

Fig. 6. Time-longitude section for the first two EOF's for realizations of 4 months of the model anomalies.

and are not significantly different from zero at a 95% confidence level. There is also a line of weaker maximum delayed in the west with respect to the reference. The slopes of these lines cannot be fitted with characteristics of Kelvin waves and first Rossby waves of the second vertical mode, which contributes to a large share of the anomalies (~50%).

4.2. *Empirical Orthogonal Functions*

The need for evaluating empirical orthogonal functions was shown in section 3. The typical duration of an "experiment" is 2 years, and this should be the length of one realization. With a 2-year duration, there are only 10 different realizations, which is not enough to have confidence into the EOFs. Because the largest lagged correlations were found (Figure 5) to be confined within 3-month lag, it is suggested that pieces of length $T = 4$ months will still contain most of the useful information and will provide 63 nearly independent realizations of the space-time variability (note that what is usually called the "spatial structure" of the EOF is here a spatial and temporal function). The first EOF includes 26% of the variance, and the second includes 11% of the variance. The first EOF shows no propagation, and the second one shows an eastward propagation superposed on a standing pattern with a sign reversal between months 2 and 3 (Figure 6). But, to a large extent, the first two EOF's can be approximated as a product $f(x)g(t)$, where $f(x)$ is close to the first EOF pattern of Figure 7*a* and $g(t)$ is its time dependence. This suggests that dependence in x and t can be separated without much statistical loss. This also results from Figure 5, which shows that the primary signal associates anomalies of one sign in the east with anomalies of the opposite sign in the west (there is, however, a slight lag, which is also found in the first EOF).

Because of this near stationarity of the EOF structure functions, there is not much loss in separating variables and seeking for more simplicity a decomposition of the signal as

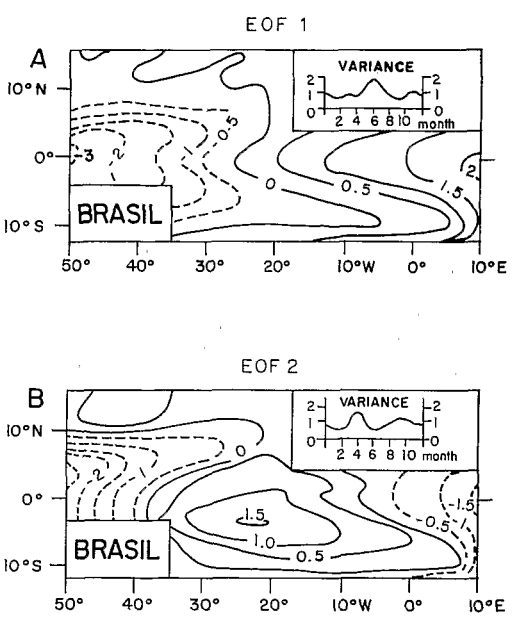

Fig. 7. Normalized spatial pattern of the first two EOFs (F_1 and F_2) of the model dynamic height anomalies. The seasonal dependence of the variance associated with the EOF is shown in the upper right corner: the x axis is the month in the calendar year, and the y axis is a normalized variance (1 corresponds to 1.7 and 0.6 (dyn cm)^2 for EOFs 1 and 2, respectively).

TABLE 1*a*. Percentage of Variance λ_i Associated with EOFs for Case I (January 1964 to December 1984)

EOF No. i	λ_i, %
1	34.0
2	12.0
3	7.2
4	5.5
5	4.2

$$h(x, t) = \sum_{k=1}^{P} \hat{a}_k F_k(x)\, G_k(t) + \text{Res} \tag{12}$$

where both F_k and G_k form a set of orthogonal functions

$$\overline{F_k(x)F_1(x)} = \delta_{k,l}$$
$$\overline{G_k(t)G_1(t)} = \delta_{k,l}\lambda_k \tag{13}$$

where the overbar denotes averages over the grid points (in x or in t) and λ_k is the variance associated with EOF k. According to what was discussed in the introduction, this is equivalent to the decomposition in EOF (equations (7) and (11)) where each month is considered as another realization (although here they are not independent). This is the classical approach described by *Lorenz* [1956] and for which uncertainty estimates are discussed by *Preisendorfer et al.* [1981]. This has also been adopted by *White et al.* [1985] for the analysis of simulations of the Pacific Ocean interannual variability presented by *Busalacchi and O'Brien* [1981]. The EOFs are ordered by decreasing importance (Table 1*a*). The first two EOFs include 46% of the variance (slightly more than was included above when the EOF was a spatial and temporal function); for higher mode number k there is a slow decrease of λ_k with mode number, and the first 11 EOFs share 80% of the total variance. The variance in the first EOF has a strong seasonal cycle similar to the seasonal cycle of the total variance, with maximum values in June and lowest values in September and between December and April (Figure 7*a*). The second EOF has maximum variance in April (Figure 7*b*) and August–September, when the first EOF has little variance.

We retain only 11 EOFs in the decomposition because higher EOFs will not be resolved with the data array of FOCAL/SEQUAL (section 4). On the other hand, only two EOFs are statistically significant, as is found using tests described by *Preisendorfer et al.* [1981]. This is also suggested by the following: when 1 single year in the time series is omitted, the first two EOF's are not modified significantly, but the higher ones change substantially, and the 21-year period (1964–1984) is not long enough for getting significant components for these modes. The years sampled by FOCAL/SEQUAL (1983–1984) include a large part of the total variance (20%, compared with 10% for an average pair of years). They account for even more of the first EOF (over 25% of its total variance). In 1984, the component of the first EOF peaks in April–May (Figure 11), but the maximum variance of the first EOF is in May or June (Figure 7*a*). However, when 1983 and 1984 are removed from the time series, patterns for the first three EOF's remain close to those in Figure 7.

The normalized spatial patterns $F_k(x)$ are also shown in Figure 7 for the first two EOF's. The large amplitudes of the first EOF are found near the equator with opposite signs in the east and the west. In the west, amplitudes are very small near 10°N with a weak reversal of sign. This suggests that

TABLE 1*b*. Correlation Coefficient $C_{I,J^i} = \overline{F_I(x)F_{J^i}(x)}$

Case	EOF 1	EOF 2
J: 228 months from January 1984 to December 1982	0.99	0.98
J: January, 1964–1984	0.95	0.78
J: April, 1964–1984	0.91	0.88
J: July, 1964–1984	0.97	0.53
J: October, 1964–1984	0.91	0.87

The overbar stands for spatial averaging, and i refers to the EOF number. I corresponds to the 252-month long time series (January 1964 to December 1984), and J corresponds to various subsets of the time series.

there is not much coherence between the anomalies on the northern side of the NECC and the swing of mass along the equator associated with the first EOF. This contrasts with the climatological seasonal cycle, where the two sides of the NECC are negatively correlated (*Garzoli and Katz* [1983], *Garzoli and Philander* [1985], these simulations). The higher-order empirical orthogonal functions have more reversals of signs and thus smaller spatial scales. These EOF patterns have been obtained by mixing all months with the assumption that the variability is not strongly seasonally dependent.

When considering time series composed of the different years for 1 given month, the patterns for the first EOF are very similar to the one in Figure 7, with correlation coefficients always larger than 0.91 (Table 1*b*). The main change is in the symmetry of the western pole with respect to the equator. It is most symmetric in July and less so in April–May, when a tongue extends south of the equator in the central Atlantic. Higher orders show stronger differences; for example, the second EOF has a different spatial structure in July than in other seasons, where it is close to the pattern for the whole year (Table 1*b*). Note that July is a month for which the variance in the second EOF is small.

Lagged correlation for the first EOF, $C(n\ \Delta t) = \overline{G_k(t_0)G_k(t_0 + n\ \Delta t)}$ also has a seasonal cycle (not shown). For $n = 2$ (lag of 2 months), the correlations are larger than 0.5 when t_0 is from April through June but weaker when t_0 is from August through September or from November through March. The periodogram for the first EOF (Figure 8*a*) has a peak near a period of 2 years and a decrease at low frequencies which is due to the filtering of these frequencies. It also decreases sharply for periods shorter than 6 months, with 92% of the variance contained at periods longer than 4 months. The decrease is not as steep for higher-order EOFs. For example, the second EOF does not have a well-defined peak at a period of 2 years, and only 85% of its variance is at periods longer than 4 months. This differs significantly from what is found for the first EOF at the 95% confidence level. To have useful functions for the analysis, a decomposition of G_k as a combination in Fourier components (here T will be 2 years) will be done as

$$G_k(t) = \sum_{l=0}^{q} a_{k,l} \cos(2\pi lt/T) + b_{k,l} \sin(2\pi lt/T) \qquad (14)$$

(we will also include a slope and a constant in the basis functions). The variance $\langle a_{k,l}\rangle^2 = \langle b_{k,l}\rangle^2$ can be estimated from periodograms, as is presented in Figure 8. For the analysis, only periods longer than 3 months are retained, and we assume that the $a_{k,l}$, $b_{k,l}$ are independent joint normally distributed variables. This is not true if anomalies propagate, in which case there are couples (k, k') for which $\langle a_{k,l}\ a_{k',l}\rangle$ will be different from zero.

5. Analysis of Proxy Data

5.1. *The Data*

In the simulations, the strongest anomalies are between May 1983 and August 1984. We will first investigate whether or not the data collected for these 2 years 1983 and 1984 cover adequately the very anomalous dynamic heights (notice that the period that we will analyze (January 1983 to December 1984) lasts longer than the extensive experiment phase of FOCAL/SEQUAL (February 1983 to September 1984). Data which should be available to the scientific community (sketch in Figure 1) include CTD data in (1) the FOCAL cruises [*Hisard and Hénin*, 1984; *Hénin et al.*, 1986; *McPhaden et al.*, 1984*b*], (2) the Transient Tracers in the Ocean (TTO) program in the western equatorial Atlantic [*Brewer et al.*, 1985], (3) "long lines" south of Abidjan [*Smethie et al.*, 1985], (4) a cross-Atlantic section at 11°30'S [*Collins*, 1984], and (5) a section in the central Atlantic Ocean [*Perkins and Saunders*, 1984]. These sections form a small core of accurate data from which

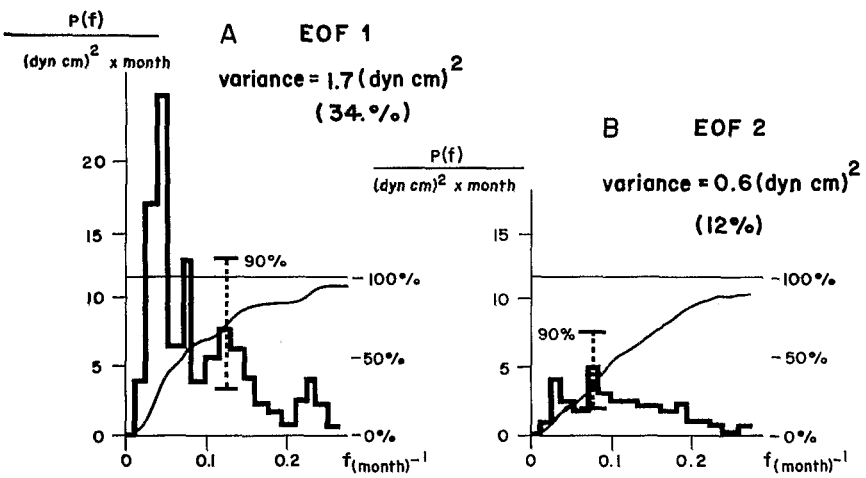

Fig. 8. Spectra of the time series associated with the first two EOFs. The spectra $P(f)$ are presented in a variance-conserving diagram (heavy solid line), one typical 90% confidence interval is shown (dashed line), and the integrated spectrum $\int P(f)\,df$ is also drawn (scale from 0 to 100%) (solid line).

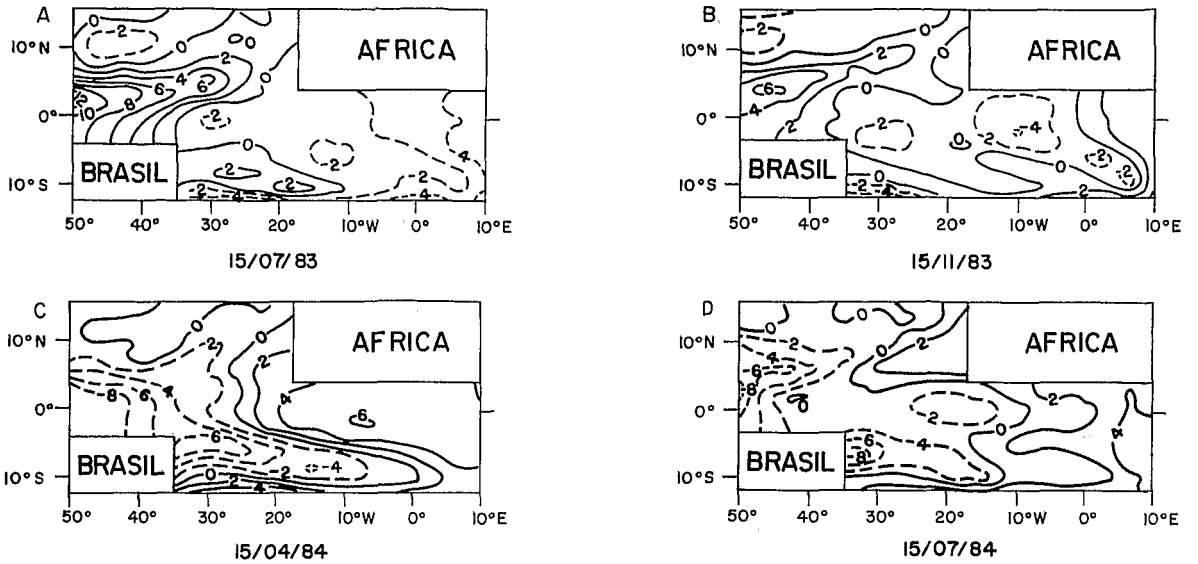

Fig. 9. Simulated dynamic height anomalies (in dynamic centimeters) at four times: (*a*) July 15, 1983; (*b*) November 15, 1983; (*c*) April 15, 1984; and (*d*) July 15, 1984.

dynamic height can be readily computed. Temperature profiles are much more numerous, and it is hoped that estimates of dynamic height will be derived from them [*Arnault*, 1984]. They include XBTs from French and American ship of opportunity programs [*Bruce and Kerling*, 1984; *Rual and Jarrige*, 1984], German data from various contributors, air-dropped XBTs at 4°W south of Ivory Coast (6 sections between May and September 1983 and 12 sections between May and October 1984) [*Houghton*, 1984] and in two surveys off Brazil [*Bruce and Kerling*, 1984]. Additional available data are the temperature messages collected in real time by meteorological centers through the Integrated Global Ocean Station System (IGOSS) international network (660 profiles were retained from this source away from the XBT routes monitored by FOCAL/SEQUAL). These messages are less accurate and are given a lesser weight in the analysis. However, it is hoped that the associated temperature profiles will be available in the future.

The cruise profiles are subsampled approximately every 2° in latitude and 4° in longitude to fit with the grid of the model, and they are attributed to day 15 of the month in which they are collected. Altogether, approximately 2000 of these subsampled profiles are available. We also include one value per month from tide gauges of the tropical Atlantic network away from western boundaries (the solution for the western boundary currents is not included in the model dynamic height). These are located at São Tome (6°40′E, 0°15′N), Penedos São Pedro e São Paulo (28°E, 0°45′N), and Ascension Island (18°W, 8°S) and on one island in Capo Verde (20°W, 14°N). It is assumed here that these additional data can be calibrated with respect to surface dynamic height. In one test, we will add the transit times measured by eight inverted echo soun-

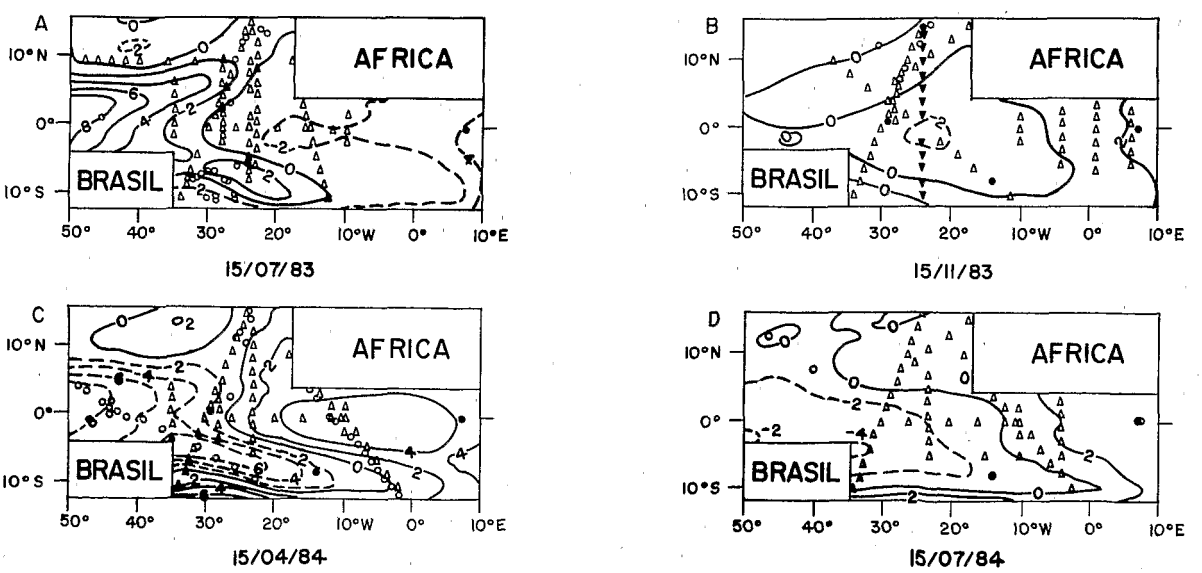

Fig. 10. Analyses of data extracted from the model at the same dates as in Figure 9. The symbols represent the positions of the data and are as follows: triangles, FOCAL/SEQUAL data; open circles, messages; and solid circles, measurements by tide gauges.

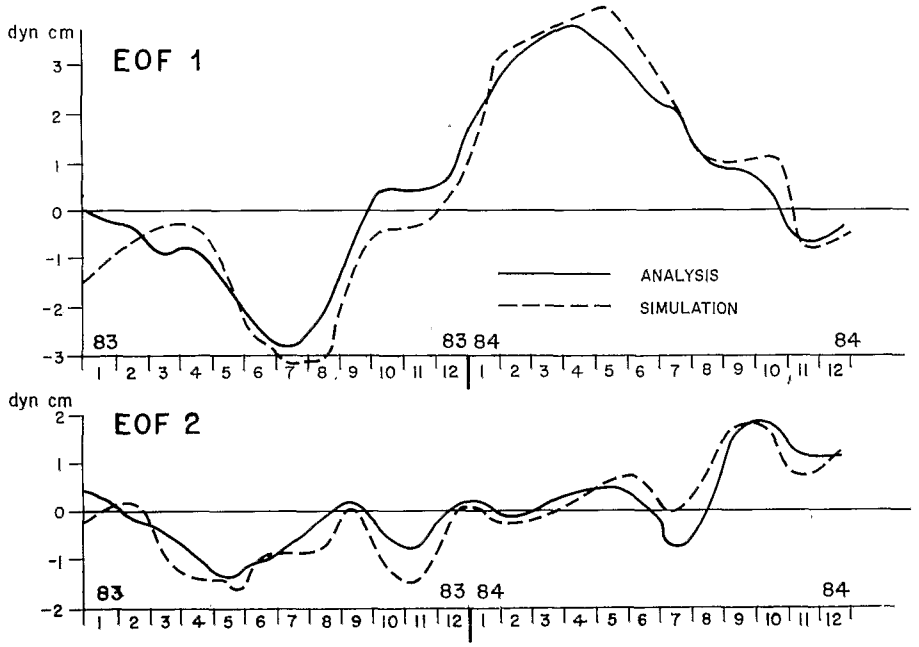

Fig. 11. Time series of the first two EOFs in 1983–1984 in the simulation (dashed line) and the analysis for the standard case (case 1 in Table 2) (continuous line).

ders (IES) located along the equator and at 3°N and 9°N along 38°30'E and 28°E [*Katz*, 1984]. These data should also be indicative of surface dynamic height [*Katz*, 1987]. The resulting data coverage is irregular (Figure 10) with highest density in the central tropical Atlantic, fewer data in the east, and large gaps in the western Atlantic Ocean (west of 35°W), the most important of those occuring in October–December 1983.

The data are extracted from the simulations at the positions of the real data (equation (5)), as

$$d_i = h_s(x_i, t_i) + \mathrm{Err}_i \tag{15}$$

where h_s is the model dynamic height and Err_i is a random noise. In the standard case, this noise represents subgrid-scale processes not part of the simulated dynamic height (rms σ_s) and experimental errors (rms σ_e) and

$$\mathrm{Err}_i = \sigma_s \varepsilon_i^1 + \sigma_e/(n)^{1/2} \varepsilon_i^2$$

where ε^1 and ε^2 are random processes wih unit variance. The number n of degrees of freedom for the experimental error is taken arbitrarily as 4 for FOCAL or SEQUAL data and 1 for messages. Visual inspection of the FOCAL sections suggests that σ_e is of the order of 2.0 dyn cm as was also found by the analysis of historical data [*Arnault*, 1984]. Scaling it as a displacement in thermocline depth (if data are temperature profiles only) yields a 7-m rms standard deviation, a likely value according to large-scale observations in 1979 [*Reverdin et al.*, 1986]. The variance not included in the first 11 EOFs (which define the signal) has a rms standard deviation of 1 dyn cm. There is also some variance at the excluded high frequencies, and σ_s is chosen as 1.5 dyn cm.

5.2. *The Analysis*

Data are estimated for the model simulations of the 2 years 1983 and 1984 and are analyzed with the optimal interpolation scheme of *Bretherton et al.* [1984] (see section 3) and with the statistics estimated in section 4. We present the comparison between the simulations and the analysis of the data at four times in 1983 and 1984 (Figures 9 and 10). July 1983 is chosen as one pole of the anomaly, and April 1984 is chosen as the other one. Obviously, many features of the model anomalies are well retained in the analysis. In July 1983 the positive anomalies in the western equatorial Atlantic extend westward north of the equator, and in April 1984 the negative anomalies in the western equatorial Atlantic extend westward south of the equator with very strong anomalies found as far as 20°W near 6°–8°S. The anomalies are smaller in the east than in the west, and the decrease between April 1984 and July 1984 is also well reproduced. However, there are some discrepancies, especially in areas with no data. The amplitudes are slightly underestimated which is also found when analyzing other realizations of the model variability, as is expected from our analysis scheme [*Davis*, 1985]. Also, in October–December 1983, the model dynamic height has produced large anomalies in the western Atlantic Ocean which do not have a counterpart in the analysis. The misfit of the analysis for these months (its difference with the model fields) is also present in the component of the first EOF which represents the largest spatial scales (Figure 11). It is interpreted as an earlier spin up of the 1984 anomaly than was really modelled. The second EOF also shows at this time a large difference from the observations. In general, the first EOF is better simulated than the second one, which has smaller amplitudes and variability at periods of 90 to 120 days (we will not argue whether these frequencies in the numerical model simulation have a counterpart in the observations, as the presence of aliasing of real higher frequencies in the winds by monthly sampling is likely).

The differences between the model and the analysis can be summarized by their overall rms standard deviation σ_d (Figure 12). Its rms value ranges between 1.1 and 2.0 dyn cm, which is small in comparison with σ_m, the observed rms deviation of the model dynamic height anomalies for 1983–1984 (2.76 dyn cm). Values of σ_d are largest for the months of November 1983

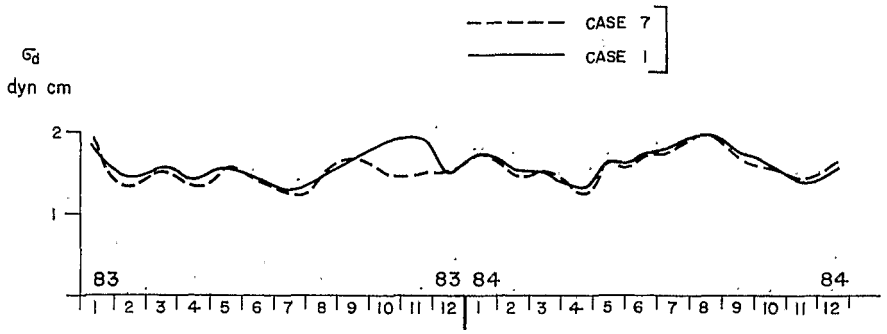

Fig. 12. Comparison in 1983–1984 of the rms standard deviation $\sigma_d = [\overline{(h_s - h_a)^2}]^{1/2}$, where the overbar denotes a spatial averaging, h_s is the simulation, and h_a is an analysis. The dashed line is for case 7 in Table 2; the continuous line is for case 1 in Table 2.

and July 1984 when the data are most scarce in the western Atlantic, and are smallest in mid-1983, when data are more evenly distributed spatially. Part of σ_d comes from the residual of the first 11 EOFs in the model anomalies (20% of the model variance, or 1 dyn cm), so that errors for the projection on the first 11 EOFs have an rms only of the order of 1 dyn cm, as is correctly forecasted by the analysis scheme. The error rms is maximum near the western end (west of 40°W), but also near Africa. It is small in the central portion of the ocean (Table 2, case 1). It peaks in late 1983 and early 1984, as was already discussed from the observed misfits between the simulation and the analysis. These larger estimated errors are the combined effect of the small data density and of the large signal expected in those areas.

We adopted previously a deterministic approach, sampling the modeled 1983–1984 period with data for those years, assuming that the simulation represents what happened in the real ocean. Alternatively, we can test the skill of the array over the 21-year-long simulation considering that it includes various possible realizations of the variability. This allows us also to compare 1983–1984 with other years and to see whether the array retains the statistical properties of the model: for instance, what are the EOFs of the analyses? Is there any propagation of signal? Is its variance seasonally dependent? First, we cut the time series into pieces of 2 years (the realizations). For each piece, the proxy data are created and then analyzed. For each realization, we compare σ_d, the rms deviation between the analysis and the model simulation, and σ_m, the rms anomaly in the model dynamic height (Figure 13). The rms anomaly σ_m has strong variations: it is large between 1968 and 1972, then small, and then very large for 1983–1984, suggesting a modulation of the magnitude of the anomaly at very low frequencies. The rms difference σ_d varies less and does not follow closely σ_m. The years sampled during FOCAL/SEQUAL, 1983–1984 yield the largest σ_d but have the smallest ratio σ_d/σ_m. Otherwise stated, errors are large, but the patterns of the anomalies are well sensed.

As a comparison, 1979–1980 has a low σ_d and a large ratio σ_d/σ_m. This implies that anomalies present in those years are very weak and that they would be poorly reproduced by the analysis. Data that were collected in 1979 [*Molinari et al.*, 1986] form an even looser array than the one tested in this study. An analysis of 1979 thermocline depth [*Reverdin et al.*, 1986] showed an anomalous deepening in May–July in the central Atlantic near 5°N which is not well reproduced in the simulations (when interpreting dynamic height anomalies as thermocline depth anomalies). The previous comment suggests that this misfit should not be considered as a major blow for the model.

With these analyses, we reconstruct a 20-year-long time series (1965–1984). These time series have much in common with the original fields. Their EOFs have very close spatial structures, and the variance is seasonally dependent. Also, the lagged cross correlations (Figure 14) have patterns similar to those shown in Figure 5. In particular, negative correlations are found at 35°W with a 3- to 4-month lead with respect to the reference at 4°W. Note that this information was not included in the statistics for the analysis, so that this reveals that the data distribution during FOCAL/SEQUAL was sufficient to sense these characteristics.

6. Discussion

The model of dynamic height between 1964 and 1984 suggests that the pattern of the anomalies in 1983–1984 is not

TABLE 2. Errors for Various Analyses Done on the 2 Years 1983 and 1984

Case	Description	σ_d,* dyn cm	Estimated Errors, dyn cm (0°, 4°W)	(0°, 28°W)	(0°, 35°W)
1	reference	1.59	1.13	0.48	0.84
2	noise halved	1.52	0.70	0.31	0.50
3	noise doubled	1.81	1.76	0.75	1.27
4	noise doubled in NW	1.61	1.21	0.50	0.87
5	without the messages	1.67	1.32	0.57	0.95
6	FOCAL cruises only	2.12	2.49	1.15	2.15
7	adding 4 data in west	1.55	1.13	0.47	0.82
8	with IES [*Katz*, 1986]	1.52	1.13	0.41	0.78

*Residual rms deviations for the difference between the simulation and the analysis, as well as estimated errors.

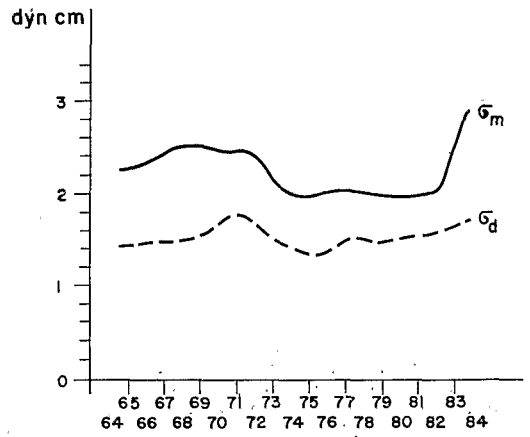

Fig. 13. Results by 2-year pieces of the simulation standard deviation σ_m and the difference between simulation and analysis σ_d.

different from what it is for other years, although in 1983–1984, there is more weight on the first EOF, which represents the largest spatial scales. We have also noticed that the strongest anomalies in 1984 occur earlier (March–May) than those for other years both in the model and its analysis with the FOCAL-SEQUAL array (for example, in 1968, where the largest anomalies are found in May–June). The model anomalies for 1983 and 1984 are very strong and of opposite sign. According to the analysis presented in the preceding section, they can be correctly sensed by the experimental array. The statistical properties of the model seem to have been adequately retained by the analysis of the data, so that possible eastward propagation of pulses along the equator will be sensed. Note that the model is relevant only for the low frequencies and that the Kelvin wave pulses described by *Katz* [1987] were not discussed here.

These conclusions rely on our confidence in the model, which we do not test here. They also depend on various assumptions on model and noise statistics. A few alternate assemblies are summarized in Table 2, giving each time the misfit between the analysis and the model simulation as well as the model estimated error in various places along the equator.

With the particular data distribution, the assumptions on the model statistics do not have too much effect on the result, although if the cutoff in the spectrum is at 4 months instead of at 3 months, the anomalies are not so well reproduced, especially for the second EOF, which varies at periods of 3–4 months. On the other hand, adequate knowledge of the noise level is a much more stringent requirement. To test that, we increase or diminish the noise level by a factor of 2 (cases 3 and 2) over the whole domain or progressively with lowest values in the southeast corner and larger values in the northwest, where it reaches 2 times the standard deviation (case 4). These alternate contingencies can be thought of as extreme possible situations: doubling the rms would still be consistent with the rms deviation at high frequencies observed on thermocline depth for 1979 [*Reverdin et al.*, 1986], and doubling it in the north-west can be interpreted as being caused by the numerous eddy structures found near the western boundary [*Bruce and Kerling*, 1984]. In both cases, with an increase of noise, the largest anomalies are still present in the analysis with a correct pattern. As may be expected, both cases show a degradation of the quality of the analysis (Table 2). Thus when dealing with real data, it is important to acquire information on the higher frequencies not retained in the analysis. Fortunately, during the FOCAL-SEQUAL field experiment, enough time series have been collected to provide the required information on the high frequencies (for example, analyses from IES travel times are presented by *Garzoli* [1984, 1987]).

Sensitivity of the quality of the analysis with respect to the data distribution is also worth investigating. We incorporated different types of data, some of which will not be so easy to use. For example, the IGOSS messages are probably not as accurate, and large errors could be present in this file. However, excluding those data results in a much larger misfit from the model dynamic height (Table 2, case 5) and gives results as poor as when the noise is double. However, note that the estimated errors did not increase as much along the equator, where data are still plentiful. Excluding other pieces of information is also detrimental to the overall quality of the analysis. On the other hand, we have noted that errors were large in the west, especially in November–December 1983, when there were no data in the west. Adding four data points (yet unknown!) to fill that gap yields a better fit to the simulation and produces smaller error estimates (Table 2, case 7; Figures 12 and 15). Adding the IES travel time records also improves the fit in the west (case 8), although to a lesser extent. This is because no IES was placed west of 40°W in the area where the largest uncertainties take place.

These comparisons suggest that we have not reached the ideal data density in the west with the FOCAL-SEQUAL data file. This conclusion holds even in the perfect case when we know perfectly the statistics of the field and with the relatively low noise level. With real data, the disagreement would be even worse in the west (we would not know the optimum statistics). It is therefore worth continuing the search for other data collected in 1983–1984 and yet unknown to us.

Up to now, analysis with real data has not been carried out on the large data sets for which this study is aimed. Analysis on real data has been done on subsets, one of which includes the seven FOCAL cruises in 1983–1984 (there were two additional cruises in 1982). *Hisard and Hénin* [1984] and *Hénin et al.* [1986] have suggested from dynamic height profiles along the equator that in early 1984 strong anomalies were present and that the surface dynamic height tilted toward

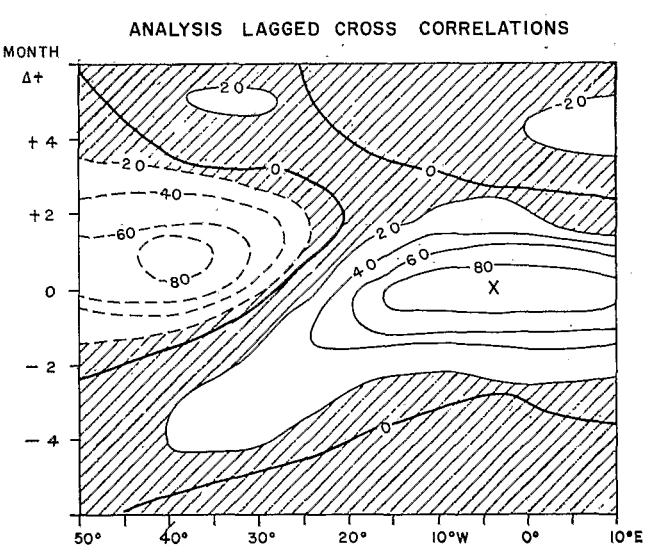

Fig. 14. Lagged cross correlations along the equator as in Figure 5 with a reference at 4°W (cross), but for the 20 years analyzed with the FOCAL-SEQUAL array (1965–1984).

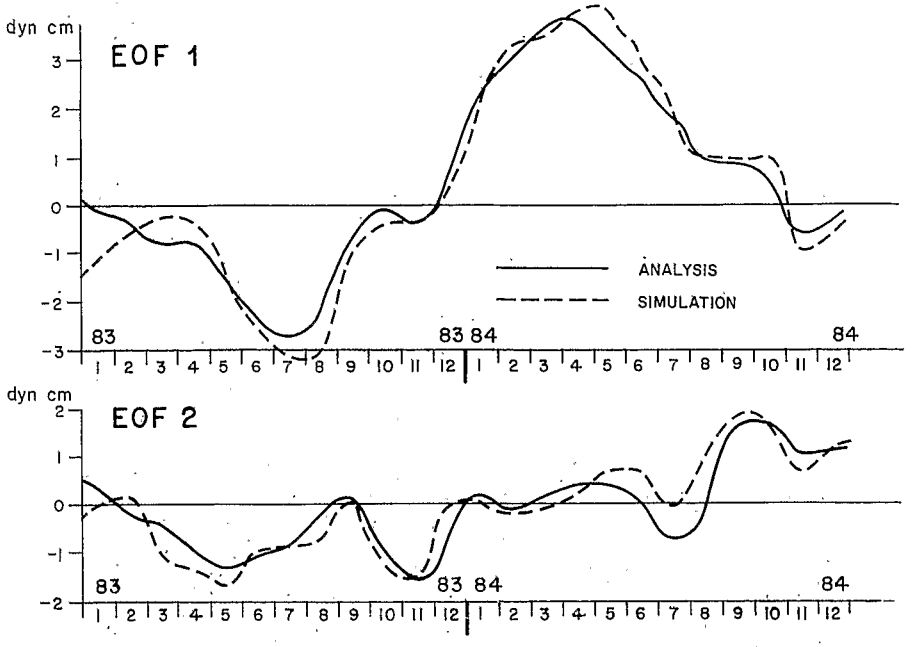

Fig. 15. Time series of the first two EOFs in 1983–1984 in the simulation (dashed line) and the analysis (solid line) for case 7 of Table 2, where 4 fake data have been added in November 1983 in the western equatorial Atlantic.

lower heights in the west, the reverse of what is commonly sensed [*Katz et al.*, 1977; *Lass et al.*, 1983]. This reversal of slope is also sustained from time series in a few locations [*Katz et al.*, 1986; *Katz*, 1987; *Weisberg and Tang*, 1987], although there are large spatial gaps between the locations of the time series and it is not obvious how they represent the larger scales. Obviously, when we perform the analysis while retaining only the FOCAL sections, the quality is downgraded with respect to the analysis from the full data set (Table 2, case 6). However, we were surprised to find that the anomalies with the largest scales, as in the component of the first EOF, are quite well retained (Figure 16). A small portion of the second EOF is even described, but the disagreement is much larger there. It is therefore not arguable that the FOCAL sections sensed the large-scale anomalies of dynamic height (at least in the model), even with this coarse temporal resolution.

The implications of these tests with data extracted from a model for the analysis of real data are that

1. To a large extent, it will be possible to extract from the data set the useful information on the variability during the field program. However, large errors remain in the west, and an increased data set in that portion of the ocean would add to the quality of the analysis. This conclusion holds for dynamic height. It is likely that results would be different for

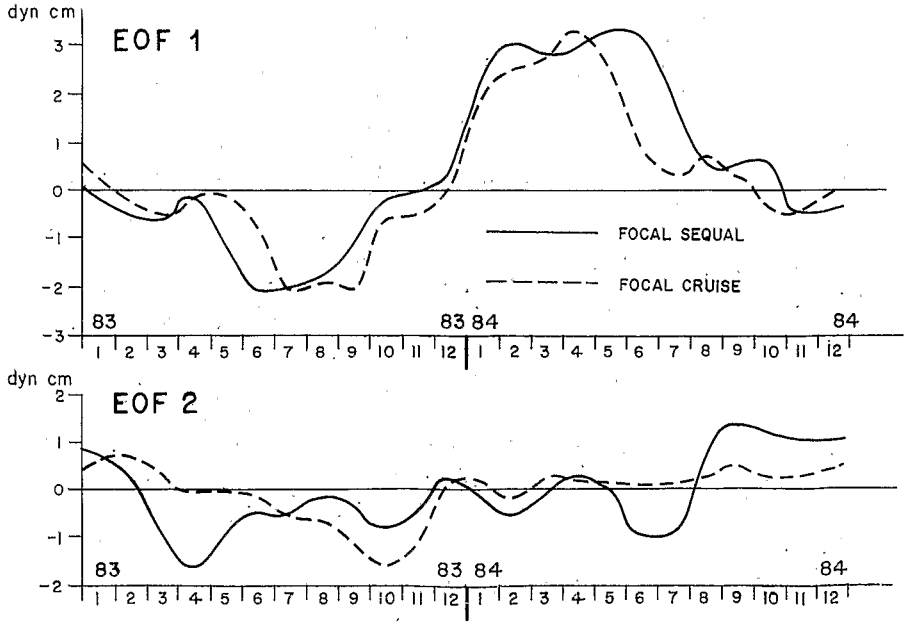

Fig. 16. Time series of the first two EOFs with analyses of reduced data sets for case 5 (continuous line) and case 6 (dashed line) of Table 2.

estimates of currents. We have not made these estimates, as we felt that the model was not as relevant for this variable [*du Penhoat and Tréguier*, 1985].

2. An increased knowledge of the high-frequency and/or small-scale variability is needed for a correct estimate of the anomalies. In that respect, inverted echo sounder travel times will be very helpful (see studies by *Garzoli* [1984, 1987] or *Katz* [1987]. These data were not included in the standard case as some calibration problems remain in interpreting them as dynamic heights [*Katz et al.*, 1986]. Also, most of them are in well-sampled areas, and in our analysis scheme they do not bring more information (note that because of this adequate coverage, intercomparison is possible at low frequencies between dynamic height computed by other means and inverted echo sounder travel times).

3. It is not controversial to describe the large-scale low-frequency variability from a few cruises as was done by *Hisard and Hénin* [1984] or with a few records (*Weisberg and Tang* (1987) or *Katz* (1987), for example). However, the conclusions that we have reached rely on the scales of the model variability. If the model dynamics were inadequate or the wind fields did not have the correct scales, the conclusions could be different. We are not at a stage where we can argue about these points. More studies remain to be done on the wind field or the model dynamics for FOCAL/SEQUAL before this can be asnwered. Fortunately, the FOCAL-SEQUAL array will be sufficient to improve our knowledge of the oceanic variability.

In conclusion, FOCAL/SEQUAL has sensed the 2 most anomalous years (1983 and 1984) among the 21 years (1964 to 1984) in the model time series. These anomalies have large spatial scales and have opposite sign in the east and the west. Anomalies of the slope across the North Equatorial Countercurrent are not as large. The two contrasting seasonal cycles 1983 and 1984 will probably be well sensed by the experimental array, and the data are likely to bring a better knowledge of the seasonal variability in the equatorial Atlantic.

Acknowledgments. This work was conceived in late 1984 during stays at the Centre de Recherches Océanographiques de Dakar-Thiaroye (Senegal) for which we are most thankful. Latter developments have been carried in Brest (antenne ORSTOM, Centre Océanographique de Bretagne), and in the Muséum National d'Histoire Naturelle in Paris. A first draft has been written while one of us (G.R.) was host on board the R/V *Marion Dufresne* of the Terres Australes et Antarctiques Françaises. Comments by S. Arnault and M. McPhaden were very helpful, and discussion with M. Cane and E. Katz were appreciated. The winds used to hindcast the dynamic height between 1964 and 1984 are courtesy of J. Servain. This paper would not have been possible without his good will and his speediness in communicating to us revised versions of the wind data set. Support by ORSTOM and CNRS is gratefully acknowledged. The analysis of the model was performed in the computer center of the Centre Français de Recherche Scientifique (CIRCE). Financial support was obtained through IFREMER grant 85/430512 and Programme National d'Etude de la Dynamique du Climat grant 950099. Figures were drafted by C. Christoforides, and help by Y. Gouriou on the model is gratefully acknowledged.

REFERENCES

Arnault, S., Variation saisonniere de la topographie dynamique et de la circulation superficielle de l'Océan Atlantique tropical, thèse de 3ème cycle, Univ. Paris 6, Dec. 14, 1984.

Bretherton, F., M. McPhaden, and E. Kraus, Design studies for climatological measurements of heat storage, *J. Phys. Oceanogr.*, *14*, 318–337, 1984.

Brewer, P., J. Sarmiento, and W. Smethie, The Transient Tracers in the Ocean (TTO) Program, The North Atlantic Study, 1981; The tropical Atlantic study, 1983, *J. Geophys. Res.*, *90*(C4), 6903–6906, 1985.

Bruce, J., and J. Kerling, Near equatorial eddies in the north Atlantic, *Geophys. Res. Lett.*, *11*, 779–782, 1984.

Busalacchi, A., and M. Cane, Hindcasts of sea level variations during the 1982–83 El Niño, *J. Phys. Oceanogr.*, *15*, 213–221, 1985.

Busalacchi, A., and J. O'Brien, Interannual variability of the equatorial Pacific in the 1960's, *J. Geophys. Res.*, *86*, 10,901–10,907, 1981.

Busalacchi, A., and J. Picaut, Seasonal variability from a model of the tropical Atlantic Ocean, *J. Phys. Oceanogr.*, *13*, 1564–1588, 1983.

Cane, M., The response of an equatorial ocean to simple wind stress patterns, II, Numerical results, *J. Mar. Res.*, *37*, 253–299, 1979.

Cane, M., and R. Patton, A numerical model for low frequency equatorial dynamics, *J. Phys. Oceanogr.*, *14*, 1853–1863, 1984.

Cane, M., and E. Sarachik, The response of a linear baroclinic ocean to periodic forcing, *J. Mar. Res.*, *39*, 651–693, 1981.

Collins, C., A trans-Atlantic upper ocean temperature section along 11°15'S in March 1983, *Geophys. Res. Lett.*, *11*, 773–774, 1984.

Davis, R., Objective mapping by least squares fitting, *J. Geophys. Res.*, *90*(C3), 4773–4777, 1985.

Düing, W., F. Ostapoff, and J. Merle, Physical oceanography of the tropical Atlantic during GATE, 117 pp. and charts, Univ. of Miami, Fla., 1980.

du Penhoat, Y., and Y. Gouriov, Hindcasts of equatorial sea surface dynamic height in the Atlantic during the Programme Français Océan Climat dans l'Atlantique Equatorial/Seasonal Response of the Equatorial Atlantic (1982–1984), *J. Geophys. Res.*, in press, 1987.

du Penhoat, Y., and A. M. Tréguier, The seasonal linear response of the tropical Atlantic Ocean, *J. Phys. Oceanogr.*, *15*, 316–329, 1985.

Garzoli, S., Modes of variability of the 1983 thermocline signal, *Geophys. Res. Lett.*, *11*, 741–744, 1984.

Garzoli, S., Forced oscillations in the equatorial Atlantic basin during the Seasonal Response of the Equatorial Atlantic program (1983–1984), *J. Geophys. Res.*, in press, 1987.

Garzoli, S., and E. Katz, The forced annual reversal of the Atlantic North Equatorial Countercurrent, *J. Phys. Oceanogr.*, *13*, 2082–2090, 1983.

Garzoli, S., and G. Philander, Validation of an equatorial Atlantic simulation model using inverted echo sounder data, *J. Geophys. Res.*, *90*(C5), 9199–9201, 1985.

Gent, P., K. O'Neill, and M. Cane, A model of the semi-annual oscillation in the equatorial Indian Ocean, *J. Phys. Oceanogr.*, *13*, 2148–2160, 1983.

Hastenrath, S., Interannual variability and annual cycle: Mechanisms of circulation and climate in the tropical Atlantic sector, *Mon. Weather Rev.*, *112*, 1097–1107, 1984.

Hellerman, S., and M. Rosenstein, Normal monthly wind stress over the world ocean with error estimates, *J. Phys. Oceanogr.*, *13*, 1093–1104, 1983.

Hénin, C., P. Hisard, and B. Piton, Observations hydrologiques dans l'Océan Atlantique équatorial (juillet 1982–août 1984), *Trav. Doc. ORSTOM*, *196*, 191 pp., 1986.

Hisard P., and C. Hénin, Zonal pressure gradient, velocity and transport in the Atlantic Equatorial undercurrent from FOCAL cruises (July 1982–February 1984), *Geophys. Res. Letters*, *11*, 761–764, 1984.

Houghton, R., Seasonal variation of the subsurface thermal structure in the Gulf of guinea, *J. Phys. Oceanogr.*, *13*, 2010–2020, 1983.

Houghton, R., Seasonal variation of the Gulf of Guinea thermal structure, *Geophys. Res. Lett.*, *11*, 783–786, 1984.

Katz, E., Dynamic topography of the sea surface in the equatorial Atlantic, *J. Mar. Res.*, *39*, 53–63, 1981.

Katz, E., Basin wide thermocline displacements along the equator of the Atlantic in 1983, *Geophys. Res. Lett.*, *11*, 729–732, 1984.

Katz, E., Seasonal response of the sea surface to the wind in the equatorial Atlantic, *J. Geophys. Res.*, in press, 1987.

Katz, E., et al., Zonal pressure gradient along the equatorial Atlantic, *J. Mar. Res.*, *35*, 293–307, 1977.

Katz, E., P. Hisard, J. M. Verstraete, and S. Garzoli, Annual changes of the zonal pressure gradient along the equator of the Atlantic Ocean in 1983/84, *Nature*, *322*, 245–247, 1986.

Kaufeld, L., The development of a new Beaufort equivalent scale, *Meteorol. Runds.*, *34*, 17–23, 1981.

Lass, H., et al., Seasonal changes of the zonal pressure gradient in the equatorial Atlantic during the FGGE year, *Oceanol. Acta*, *6*, 3–11, 1983.

Legler, D., and J. O'Brien, Atlas of the tropical Pacific wind stress climatology 1971–1980, 187 pp., Fla. State Univ., Tallahassee, 1985.

Lighthill, M., Dynamic response of the Indian Ocean to the onset of the south west monsoon, *Philos. Trans. R. Soc. London, Ser. A, 265*, 45–93, 1969.

Lorenz, E., Empirical orthogonal functions and statistical weather prediction, *Sci. Rep. 1*, Statis. Forecast Proj., Mass. Inst. of Technol., Cambridge, 1956.

Madden, R., and P. Julian, Description of global-scale circulations cells in the tropics with a 40–50 day period, *J. Atmos. Sci., 29*, 1109–1123, 1972.

McCreary, J., A linear stratified ocean model of the equatorial Undercurrent, *Philos. Trans. R. Soc. London, Ser. A, 278*, 603–635, 1981.

McCreary, J., J. Picaut, and D. Moore, Effects of remote annual forcing in the eastern tropical Atlantic Ocean, *J. Mar. Res., 42*, 45–81, 1983.

McPhaden, M., G. Reverdin, J. Merle, Y. du Penhoat, and A. Kartavtseff, Objective analysis of simulated equatorial Atlantic Ocean data on seasonal time scales, *Deep Sea Res., 31*, 551–569, 1984*a*.

McPhaden, M., M. Fieux and J. Gonella, Meanders observed in surface currents and hydrography during an equatorial Atlantic transect, *Geophys. Res. Lett., 11*, 757–760, 1984*b*.

Merle, J., Atlas hydrologique saisonnier de l'Océan Atlantique intertropical, *Trav. Doc. ORSTOM, 82*, 184 pp, 1978.

Merle, J., Seasonal heat budget in the equatorial Atlantic Ocean, *J. Phys. Oceanogr., 10*, 464–469, 1980.

Merle, J., and S. Arnault, Seasonal variability of the surface dynamic topography in the tropical Atlantic Ocean, *J. Mar. Res., 43*, 267–288, 1985.

Molinari, R., et al., A synthesis of the First GARP Global Experiment (FGGE) in the equatorial Atlantic Ocean, *Prog. Oceanogr., 16*, 91–112, 1986.

Moore, D., et al., Equatorial adjustments in the eastern Atlantic, *Geophys. Res. Lett., 5*, 637–640, 1978.

Murakami, M., Large scale aspects of deep convective activity over the GATE, area, *Mon. Weather Rev., 107*, 994–1013, 1979.

Perkins, H., and K. Saunders, Atlantic equatorial sections during July 1983, *Geophys. Res. Lett., 11*, 769–772, 1984.

Philander, G., and R. Pacanowski, The generation of equatorial currents, *J. Geophys. Res., 85*, 1123–1136, 1980.

Philander, G., and R. Pacanowski, Simulation of the seasonal cycle in the tropical Atlantic Ocean, *Geophys. Res. Lett., 11*, 802–804, 1984.

Philander, G., and R. Pacanowski, A model of the seasonal cycle in the tropical Atlantic Ocean, *J. Geophys. Res., 91*(C12), 11,727–11,739, 1986.

Picaut, J., Propagation of the seasonal upwelling in the eastern equatorial Atlantic, *J. Phys. Oceanogr., 13*, 18–37, 1983.

Picaut, J., J. Servain, P. Lecomte, M. Seva, S. Lukas, and G. Rougier, Climatic atlas of the tropical Atlantic Ocean wind stress and sea surface temperature 1964–1979, 467 pp., Univ. of Hawaii, Honolulu, 1985.

Preisendorfer, R., F. Zwiers, and T. Barnett, Foundations of principal component selection rules, *SIO Ref. Ser. 81-4*, 192 pp., Scripps Inst. of Oceanogr., La Jolla, Calif., 1981.

Reverdin, G., R. Molinari, and Y. du Penhoat, Objective analysis of thermocline depth distributions obtained in the tropical Atlantic Ocean during FGGE, 1979, *Deep Sea Res., 33*, 43–53, 1986.

Rual, P., and F. Jarrige, Tropical Atlantic thermal structure along the Europe-Brasil ship line, *Geophys. Res. Lett., 11*, 775–778, 1984.

Servain, J., Réponse océanique à des actions éloignées du vent dans le Golfe de Guinée en 1967–1968, *Oceanol. Acta, 7*, 297–307, 1984.

Servain, J., J. Picaut, and A. Busalacchi, Interannual and seasonal variability of the tropical Atlantic Ocean depicted by sixteen years of sea surface temperature and wind stress, in *Coupled Ocean-Atmosphere Models, 16th Liège Colloquium on Ocean Hydrodynamics*, edited by J. C. Nihoul, pp. 211–237, Elsevier, New York, 1985.

Smethie, W., T. Takahashi, D. Chipman, and J. Ledwell, Gas exchange and CO_2 flux in the tropical Atlantic Ocean determined from ^{222}Rn and pCO_2 measurements, *J. Geophys. Res., 90*(C4), 7005–7020, 1985.

Weisberg, R., SEQUAL/FOCAL: Editorial, *Geophys. Res. Letters, 11*, 713–714, 1984.

Weisberg, R., and T. Tang, Equatorial Atlantic thermocline response to wind forcing, *J. Geophys. Res., 90*, 7117–7128, 1985.

Weisberg, R., and T. Tang, On the response of the equatorial thermocline in the Atlantic Ocean to the seasonally varying trade winds, 2, *J. Geophys. Res.*, in press, 1987.

White, N., S. Pazan, and Li B., Processes of short-term climatic variability in the baroclinic structure of the interior western tropical north Pacific, *J. Phys. Oceanogr., 15*, 386–402, 1985.

Y. du Penhoat, Antenne ORSTOM, Centre IFREMER, B. P. 337, 29273 Brest, France.

G. Reverdin, LODYC, Centre National de Recherche Scientifique, Université Paris VI, 4 Place Jussieu, 75005 Paris, France.

(Received July 7, 1986;
accepted August 2, 1986.)